Quasi-ideal feedback-loop supercurrent diode

Giorgio De Simoni* and Francesco Giazotto†
NEST, Istituto Nanoscienze-CNR and Scuola Normale Superiore, Pisa I-56127, Italy

(Received 23 February 2024; revised 16 May 2024; accepted 22 May 2024; published 25 June 2024)

We suggest using a device called the bootstrap superconducting quantum interference device (BS SQUID) to break the reciprocity in charge transport. This device uses magnetic flux backaction to create a nonreciprocal current-voltage characteristic, which results in a supercurrent rectification coefficient of up to approximately 95%. The BS SQUID works as a quasi-ideal supercurrent diode (SD) and maintains its efficiency up to about 40% of its critical temperature. The external magnetic flux can be used to adjust or reverse the rectification polarity. Finally, we discuss the finite-voltage operation regime of the SD and present a possible application of our device as a half- and full-wave signal rectifier in the microwave regime.

DOI: 10.1103/PhysRevApplied.21.064058

I. INTRODUCTION

A charge diode is an electronic device with two terminals that allows an electric current to flow in only one direction while blocking it in the opposite direction, making it a nonreciprocal device. This property is due to the lack of spatial symmetry, which is intentionally broken during device design and fabrication, e.g., in systems such as p-n and Schottky junctions. The efficiency of a diode is measured by the saturation current, which determines its degree of ideality through the amplitude of the maximum reverse current when the diode is reverse biased. These semiconductor devices have a wide range of applications, from detecting and generating photons to signal rectification, and they are essential components of semiconducting electronics. In addition to the latter, superconducting electronics has developed significantly due to its superior energy efficiency and larger operation frequency. This development has been made possible by demonstrating many superconducting equivalents of semiconductor devices [1–7], including systems that implement nonreciprocal dissipationless Cooper-pair transport. A supercurrent diode (SD) is a superconducting circuital element that has different amplitudes of positive (I^+) and negative (I^-) switching critical currents. Similar to the semiconducting case, the ideality of an SD is crucially determined by a rectification coefficient $\eta = (|I^+| - |I^-|)/(|I^+| + |I^-|)$ that ranges from 0 (no rectification) to 1 (perfect rectification). Thus, an ideal SD with $\eta = 1$ can sustain a supercurrent in one direction and just a *normal* dissipative current in the other. Although the idea of realizing supercurrent rectifiers is in itself not new [8] and despite a recently renewed [9] and intense research effort, a platform of choice to realize SDs has not been identified yet. Indeed, nonreciprocal supercurrent transport, due to inversion and time-reversal symmetry breaking, was demonstrated in relatively exotic materials and heterostructures [9–19]. Several mechanisms, mainly exploiting spin-orbit coupling and magnetic effects, have been proposed to implement rectification in superconducting films and Josephson junctions (JJs) [19–42]. Nonetheless, the race to maximize the supercurrent rectification efficiency has driven the demonstration of devices with η values in the range of a few tens percent [38], and barely approaching 90% in Nb devices exploiting current backaction mechanisms [42]. Present technology SDs are, therefore, far from ideal. This severe performance limitation, together with the use of complex material systems and the exploitation of physical mechanisms that are hardly modeled and engineered, is holding back the application of SDs in practical applications, limiting the design of new platforms based on their exploitation.

Here, we propose and analyze a superconducting quantum interference device (SQUID) that utilizes a feedback loop to implement a magnetic flux backaction. This results in the device's current-voltage characteristics that strongly favor one direction over the other. By adjusting the external magnetic flux Φ_{ex}, we can unbalance the critical currents I^+ and I^- to achieve a nearly perfect rectification coefficient, which allows us to implement a quasi-ideal SD.

II. BOOTSTRAP SQUID SUPERCURRENT DIODE

In their more conventional implementation, which we assume in the following, SQUIDs consist of two tunnel JJs closed on a superconducting loop, whose switching

*Corresponding author: giorgio.desimoni@nano.cnr.it
†Corresponding author: francesco.giazotto@sns.it

current is modulated by the magnetic flux Φ threading the device with a periodicity equal to the magnetic flux quantum, $\phi_0 = h/2e$ [43]. Thanks to their excellent sensitivity, SQUIDs are at the core of state-of-the-art cryogenic magnetometers, inductively coupled current amplifiers [43–48], and are often included in larger systems designed to perform signal-processing applications [49]. The use of SQUIDs as supercurrent rectifiers has been recently shown in systems with a large inductance [50,51], which on one side is crucial to produce the rectifying behavior, while on the other side limits the maximum achievable rectification, due to the reduced amplitude of the switching current modulation with the flux [43]. Our approach relies on coupling the SQUID loop with a feedback coil. Feedback inductors are conventionally bootstrapped in the control and readout circuitry of SQUID amplifiers and magnetometers to reduce the noise contribution from the room-temperature preamplifiers and increase their linear dynamic range. [52–62]. Similarly, in our approach, a feedback coil with inductance L_F is wired in series and inductively coupled via a mutual inductance coefficient M to a current-biased SQUID, consisting of a ring of inductance L_S and a left and a right JJ having critical currents and phase drops I_L and I_R and φ_L and φ_R, respectively. The total magnetic flux Φ threading the loop is the sum of the external flux $\Phi_{\rm ex}$ and of the flux induced by the feedback loop $\Phi_F = MI$, where I is the bias current flowing through the interferometer. It follows that Φ is a function of I, which is common to both the SQUID and the feedback coil. This results in a flux backaction mechanism, which can be exploited to implement the supercurrent rectifying mechanism. The circuital scheme of such a bootstrap SQUID (BS SQUID) is depicted in Fig. 1(a).

To understand where the rectification properties arise from, it is necessary to resort to the resistively shunted Josephson junction (RSJ) equations of the SQUID [43]:

$$\begin{aligned}
\frac{I}{I_0} &= (1-\alpha_i)\sin(\varphi_L) + (1+\alpha_i)\sin(\varphi_R),\\
\frac{2j}{I_0} &= (1-\alpha_i)\sin(\varphi_L) - (1+\alpha_i)\sin(\varphi_R),\\
\delta\varphi &= \varphi_L - \varphi_R = \frac{2\pi\Phi}{\phi_0} + \pi\beta_l\frac{(j-\alpha_l I)}{I_0},\\
I_0 &= \frac{I_L + I_R}{2},\\
L_S &= L_L + L_R. \qquad (1)
\end{aligned}$$

In Eq. (1), we introduced the coefficients $\alpha_i = (I_R - I_L)/(I_R + I_L)$, $\alpha_l = (L_R - L_L)/(L_R + L_L)$, and $\beta_l = (2L_S I_0)/(\Phi_0)$ accounting for the difference between the critical current of the left and right junction, the asymmetries in the inductance (L_L and L_R) of the two arms of the loop, and the SQUID screening, respectively. j, which is defined as the difference between the current across each JJ, is the so-called circulating current of the SQUID. I^+ and I^- are calculated from Eq. (1) by maximizing and minimizing I over $\delta\varphi$, respectively. By expanding the fluxoid

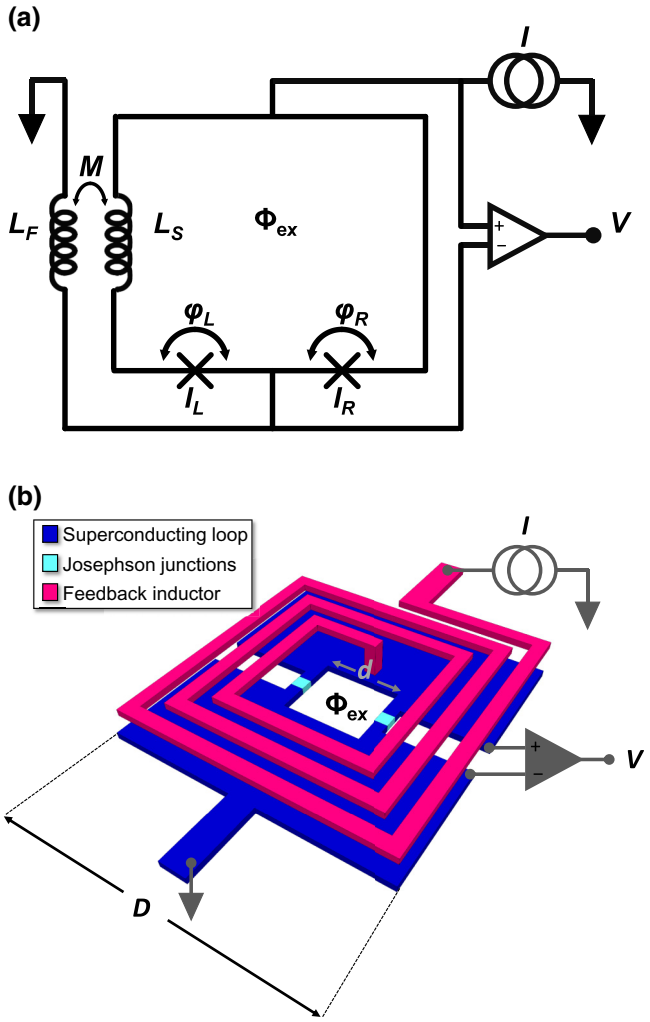

FIG. 1. Supercurrent diode based on the magnetic flux backaction: the BS SQUID. (a) Circuital scheme of a supercurrent diode based on the magnetic flux backaction induced by bootstrapping an external coil. The SQUID is a superconducting ring with total inductance L_S, closed on a left and right Josephson junction, with critical current and phase drop I_L, φ_L, and I_R, φ_R, respectively. The SQUID is connected in series and inductively coupled via a mutual inductance M to a feedback inductor, with inductance L_F. The series of the SQUID and the inductor realizes the BS SQUID, which is biased with a current I. The output signal of the BS SQUID (V) is measured at the ends of the SQUID. (b) Sketch of a possible BS SQUID implementation: the SQUID (represented in blue) is realized in a *washer* geometry and is assumed to have D and d as lateral sizes for the whole device and the hole, respectively. The feedback inductance (pink) is assumed to be an electrically insulated squared superconducting spiral overlapping the SQUID. The Josephson junctions are represented in light blue.

quantization relation

$$\varphi_L - \varphi_R = \frac{2\pi}{\phi_0}(\Phi_{\rm ex} + MI) + \pi\beta_l \frac{(j - \alpha_l I)}{I_0} \qquad (2)$$

to account for the flux contribution from the feedback inductor, we observe that the latter is mathematically equivalent to unbalancing the inductance of the SQUID arms. This is known to result in a skewing of the positive $I^+(\Phi_{\rm ex})$ and negative $I^-(\Phi_{\rm ex})$ critical current versus flux characteristics in opposite magnetic flux directions, thereby causing a nonreciprocal behavior and a supercurrent diode effect at fixed external flux. We note that the introduction of an asymmetry in the SQUID arms inductances can be exploited to implement or tune an SD [50]. Nonetheless, it is worth emphasizing that $|\alpha_l|$ is by definition bound to 1 and that the $I^{+,-}(\Phi_{\rm ex})$ skewness can be enhanced by increasing the total SQUID inductance, but at the cost of damping the amplitude of the $I^{+,-}(\Phi_{\rm ex})$ swing. It is possible to achieve a rectifying behavior by using the construction parameter of the SQUID inductance, but this behavior is modest. On the other hand, introducing the feedback coil creates an additional capability to control the mutual inductance coefficient, denoted as M, which is still proportional to L_S and can be adjusted through the value of L_F. This provides the opportunity to modify the skewness of the BS SQUID $I^{+,-}(\Phi_{\rm ex})$ without significantly affecting the amplitude of their oscillation.

To illustrate this statement, we assume that our BS SQUID has a *washer* geometry, shown in Fig. 1(b), with the feedback inductor, comprising a spiral with n coils, overlapped onto the SQUID. It can be shown [63,64] that, by neglecting the parasitic inductance associated with the Josephson junctions, it holds

$$L_S \simeq 1.25\mu_0 d,$$
$$M \simeq nL_S = \frac{n\beta_l\Phi_0}{2I_0}, \qquad (3)$$

where μ_0 is the vacuum magnetic permeability, and d is the lateral size of the SQUID hole. It is worth noting that, with this geometric choice, M is proportional to the product $n \times L_S$ and $(n \times \beta_l)$. The number of coils that can be overlapped to the SQUID is a function of the washer lateral size D, while L_S is proportional only to its inner size d. This results in the possibility of increasing the mutual inductance coefficient without increasing the SQUID inductance. In turn, this allows the skewness of the $I^{+,-}(\Phi_{\rm ex})$ of the BS SQUID to be increased without significantly affecting the critical-current modulation amplitude.

III. RECTIFICATION PERFORMANCE

Figure 2(a) shows the normalized values I^+ and I^- versus $\Phi_{\rm ex}$ for selected values of n between 2 and 40, when

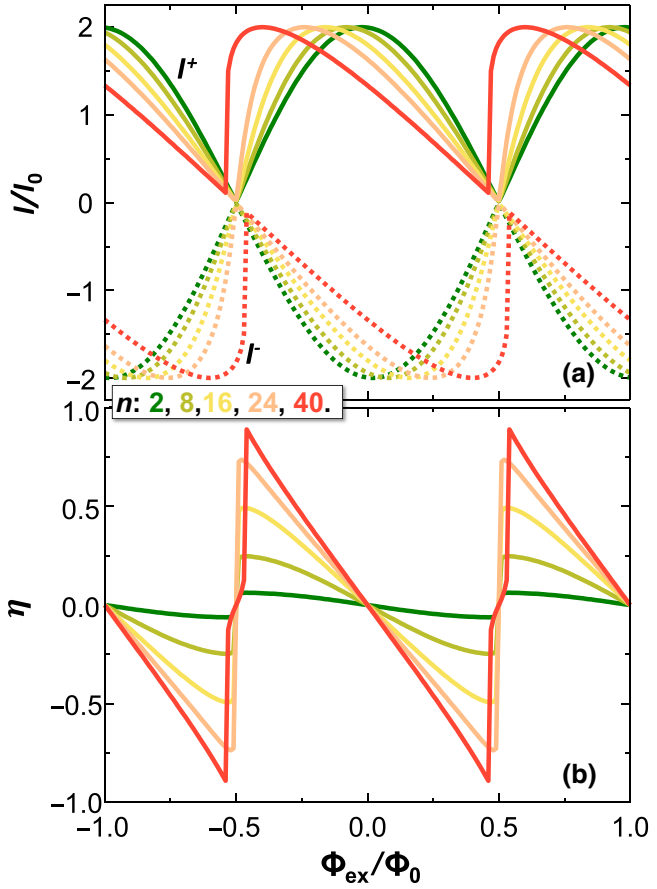

FIG. 2. BS SQUID as supercurrent diode. (a) Positive I^+ (solid curves) and negative (I^-, dashed curves) normalized switching current of a *washer* BS SQUID versus external magnetic flux $\Phi_{\rm ex}$ for selected values of the number of windings n of the feedback inductor. The BS SQUID is assumed to have identical Josephson junctions ($\alpha_i = 0$) and symmetrical inductance of the arms ($\alpha_l = 0$). The screening parameter β_l is set to 0.01. (b) Rectification coefficient η versus $\Phi_{\rm ex}$ calculated from the switching current characteristics of (a).

$\beta_l = 0.01$ and $\alpha_i = \alpha_l = 0$. Due to the low value of the screening parameter, at low winding numbers of the feedback coil (e.g., dark green curve), the $I^{+,-}(\Phi_{\rm ex})$ is almost equivalent to that of a perfectly symmetric SQUID, with a negligible skewing and with an almost full-span (approximately 2) modulation amplitude (the latter is limited only by I^+ and I^- never being exactly 0). By increasing n, the maxima of $|I^+|$ ($|I^-|$) are progressively pulled toward negative (positive) values of the magnetic flux while the minima (maxima) remain almost locked in the original position. These characteristics yield the aforementioned skewing of the $I^{+,-}(\Phi_{\rm ex})$, which is the key to achieving an efficient SD effect, and are present up to $n \sim 40$. This results in a strong and tunable supercurrent rectifying behavior, whose amplitude and sign can be controlled by external magnetic flux. This can be well appreciated by plotting η versus $\Phi_{\rm ex}$ for the same selected values of n

[see Fig. 2(b)]: the BS SQUID exhibits a periodic modulation of the rectification coefficient, which changes its sign at $\Phi_{ex} = N(\Phi_0/2)$, with $N = 0, \pm 1, \pm 2 \ldots$. This peculiar feature, which has been reported so far in just a few cases [13,17,50,65–68], can be exploited to reverse the polarity of the device during its operation. Furthermore, by increasing n, the maximum value of η increases as well due to the maxima of $|I^+|$ and $|I^-|$ being pulled in different magnetic flux directions. For $n \lesssim 40$, η reaches its maximum value, which is just slightly lower than 1.

It is impossible to achieve ideal rectification due to the requirement of a low, but nonzero, value of the SQUID inductance. However, we believe that if we can optimize the inductances or implement the device concept differently, we might be able to improve the rectification performance beyond what is shown in this work and closer to the ideality limit. In our geometry, when $n \gtrsim 40$, the excessive distortion of the $I^{+,-}(\Phi_{ex})$ causes η to stop increasing. This is mainly because the minima of $|I^+|$ and $|I^-|$ are finally unblocked and rising, as shown by the red curve in Fig. 2. It is worth emphasizing that our model assumes for the JJs a sinusoidal current-phase relation. This requirement is particularly relevant in determining the almost perfect rectification properties of the device, as the latter relies on a current-flux relationship that is almost 0 at certain magnetic flux values. This cannot be achieved when the spectral content of the Josephson junction current-phase relation is increased, because the expected effect of this is that each harmonic cancels out at different flux values. Therefore, the predictions of our model remain valid as long as the tunnel-type Josephson junctions maintain their ideality, and they cannot be automatically extended to interferometers based on generalized JJs, such as nanoconstrictions or superconductor-normal metal-superconductor junctions. In this regard, in Sec. IV, we will address, as an example, a case of implementation of the BS SQUID based on short and diffusive junctions.

In Fig. 3(a), we plot the rectification efficiency maximum value η_M versus n and β_l. The hyperbolic profile of the η_M intensity levels shows how it is essentially controlled by the mutual induction parameter M: η_M grows both as n and β_l increase until it reaches the maximum value of approximately 90% when $\beta n \sim 0.35$. Above such a threshold, η_M decreases due to the excessive distortion of the $I^{+,-}(\Phi_{ex})$ s. Figures 3(b) and 3(c) show $I^{+,-}$ and η versus Φ_{ex}, respectively, calculated by setting $\beta_l = 0.0098$ and $n = 36$ in our model. In this spot, η_M reached its maximum (approximately 0.96), a value close to the ideality limit and among the highest reported. Based on this remarkable result and their constructive simplicity, we believe that BS SQUIDs are excellent candidates for implementing superconducting platforms requiring supercurrent rectification. Interestingly, the evolution of η_M due to a variation of either β_l or n follows a similar and almost identical functional form [see Fig. 3(d), solid-black and red-dashed lines], thereby confirming M as the leading parameter in determining the rectification performance. Although changing β_l (n) at constant n (β_l) results in a

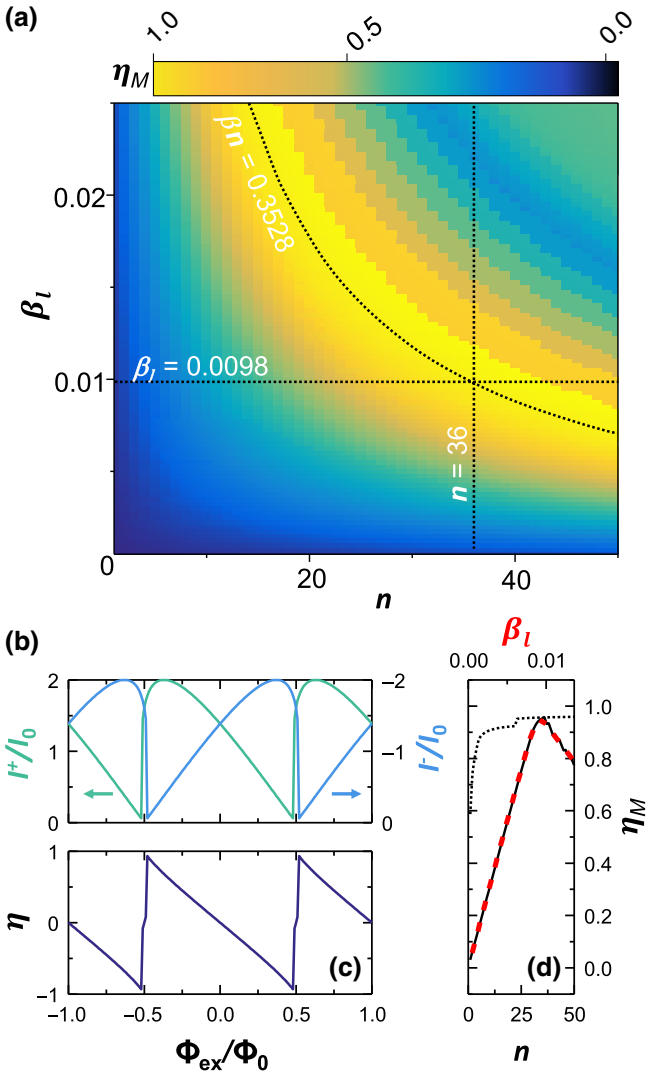

FIG. 3. Characterization of maximum rectification. (a) Maximum value of the rectification η_M versus winding number of the feedback inductance n and screening parameter β_l of a perfectly symmetrical BS SQUID. Dashed black curves highlight the cut lines at constant $\beta_l = 0.098$, $n = 36$, and $\beta_l n = 0.3526$. Where such cut lines cross, maximum rectification is achieved, in particular, along the latter η_m remains almost constant. (b) Plot of I^+ (left scale) and $|I^-|$ (right scale) versus Φ_{ex}, calculated at $n = 36$ and $\beta_l = 0.0098$, corresponding to the cross point of the cut lines of (b). (c) η versus Φ_{ex} calculated for the same parameter choice of (b), i.e., where maximum and minimum supercurrent rectification are achieved (at $\Phi_{ex} \sim \pm 0.5\Phi_0$). (d) Plot of η_m along the cut lines of (a), versus β_l (dashed red line, top scale) and n (short-dotted and continuous black lines, bottom scale). The red dashed line is the plot of η_M calculated along the $n = 36$ cut line. The short-dotted line is the plot of η_M calculated along the $\beta_l n = 0.3528$ cut lines. The continuous black line is the plot of η_M calculated along the $\beta_l = 0.0098$ cut line.

fast decrease of the rectification coefficient, it is instead almost constant if the product $\beta_l \times n$ is kept constant, with $25 \lesssim n \lesssim 50$. When $n \lesssim 25$, the rectification drops again due to a low magnetic coupling and the resulting scarce backaction [see Fig. 3(d), dotted-black line].

IV. IMPACT OF TEMPERATURE AND DEVICE IMPERFECTIONS ON THE RECTIFICATION EFFICIENCY

The following discusses the impact of temperature and device imperfections, due to fabrication limits, on the rectification efficiency of the BS SQUIDs.

To evaluate the resilience of the supercurrent rectification capability of BS SQUIDs to the temperature it is necessary to consider the temperature dependence of the critical current of the Josephson junctions. The latter is described by the Ambgaokar-Baratoff relation (AB) [69–71],

$$\frac{I_{L,R}(T)}{I_0} = \frac{\Delta(T)}{\Delta_0}\tanh\left(\frac{\Delta(T)}{2k_BT}\right), \tag{4}$$

where I_0 is the zero-temperature critical current, $\Delta(T)/\Delta_0$ is the universal Bardeen-Cooper-Schrieffer temperature-dependent amplitude of the superconducting energy gap [71] of the superconducting SQUID loop normalized over the zero-temperature superconducting gap $\Delta_0 = \Delta(T = 0)$, and k_B is the Boltzmann constant. Although in our model we take into account the SQUID inductance (and mutual inductance) through the screening parameter β_l, to compute the temperature response of the BS SQUID we decided to keep constant the inductance of the loop ($L_S = \beta_{l0}\Phi_0/2I_0$, with $\beta_{l0} = 0.0098$) and the mutual inductance ($M = nL_S = 36 \times L_S$). In the case in which the kinetic inductance of the SQUID can be neglected, this choice provides more physical insight since L_S and M are determined by geometric parameters, which remain constant in temperature. At the same time, β_l varies due to its dependence on $I_{L,R}(T)$.

Figure 4(a) shows the positive and the negative switching currents of the BS SQUID versus external magnetic flux at selected values of T. Following from the temperature evolution of $I_{L,R}(T)$ [see Fig. 4(c), black-dashed curve], the amplitude of the switching current modulation remains constant up to approximately $0.4T_C$, above this threshold it decreases to vanish at T_C. In particular, the modulation amplitude is about one half of its zero-temperature value at $T = 0.7T_C$, and approximately $\frac{1}{4}$ at $T = 0.9T_C$. Through the impact of $I_C(T)$ on β_l, the skewness of the curves is also almost preserved up to the same temperature, above which it is progressively reduced, resulting in a symmetrization of the positive and negative characteristics. This is directly reflected in the rectifying behavior of the device. In Fig. 4(b) we plot η versus Φ_{ex}

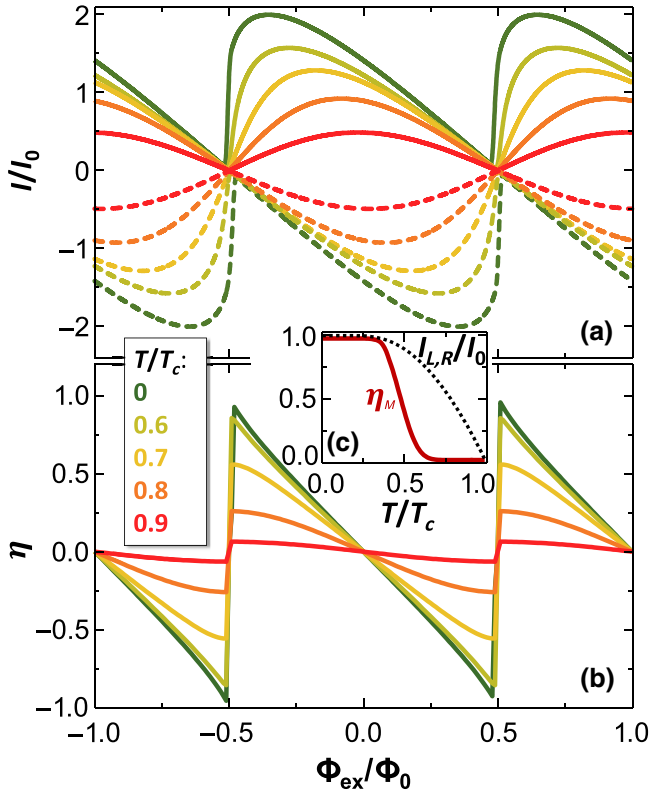

FIG. 4. Impact of the temperature. (a) I^+ (solid curves) and I^- (dashed curves) versus Φ_{ex} for selected values of the temperature T, between 0 and 0.9 T_C, calculated for a perfectly symmetrical BS SQUID with $\beta_{l0} = 0.0098$ and $n = 36$. (b) Rectification coefficient η versus Φ_{ex} for the same values of T selected for (a). (c) Maximum rectification coefficient η_M (solid red curve) and Josephson critical current $I_{L,R}$ (dashed black line) versus temperature T.

for the same values of T selected for Fig. 4(a). Although the pattern of η remains essentially unchanged as the temperature rises, its amplitude decreases accordingly with the evolution of the $I^{+,-}(\Phi_{ex})$ characteristics. It is worth noting that, due to the double impact of the reduction of $I_{L,R}$ on both the maxima of $|I_S^{+,-}|$ and on β_l, the reduction of η_M with the temperature is much faster than that of $I_{L,R}$, resulting in $\eta_M \sim 0.5\eta_M(T = 0)$ at $T = 0.7T_C$, but $\eta_M \sim 0.25\eta_M(T = 0)$ already at $T = 0.8T_C$. This is well appreciated through the comparison of $\eta_M(T)$ (red-solid curve) and $I_{L,R}(T)$ shown in Fig. 4(c). On this point, it is relevant to emphasize that this characteristic results in the interesting feature of obtaining an almost constant rectifying behavior up to $T \sim 0.4T_C$, i.e., where $I_{L,R}(T)$ is only marginally affected by heating. Furthermore, the supercurrent rectification is exploitable up to a temperature very close to the critical one, with η_M still about 5% at $T \sim 0.9T_C$.

Our model includes two parameters, α_i and α_l, to account for imperfections in the device. These

imperfections arise from asymmetries in the critical current of the left and right JJ, which can be caused by differences in junction area or tunnel barrier resistivity. Additionally, an unbalanced inductance between the two arms of the SQUID can also impact the device. However, we will discuss that this does not significantly affect the rectification properties of the BS SQUID. It is worthwhile to note that having good symmetry between the JJs is a major requirement for optimal device performance. Figure 5(a), shows the modification of the $I^{+,-}(\Phi_{ex})$ characteristics, calculated at $T = 0$ for $\beta_l = 0.0098$ and $n = 36$, when α is raised from 0 to 0.95. As conventionally observed in SQUIDs, a sizable difference between the critical currents of the JJs results in a suppression of the ability of the device to interfere and in the following suppression of the visibility of the modulation of $I_S+,-$ with the flux. This translates into an increasingly smoother $\eta(\Phi_{ex})$ relation as α_i is raised [see Fig. 5(b)]. There are two sides to the mechanism being discussed. On the one hand, it can be used positively by introducing a slight asymmetry between the junctions to widen the rectification sweet spot and reduce the device's sensitivity to flux noise. On the other hand, this comes at the cost of a severe drop in the rectification coefficient, as shown in Fig. 5(c) (violet-solid curve). Therefore, it is necessary to have excellent control over the symmetry of the BS SQUID junctions when designing and creating these devices. This is the most pivotal parameter that needs to be taken care of.

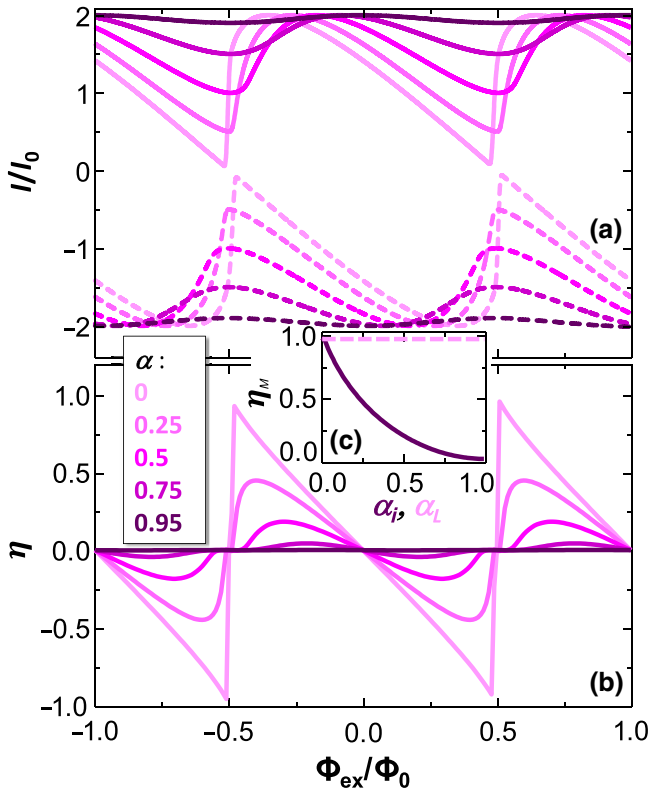

FIG. 5. Impact of device imperfection. (a) I^+ (solid curve) and I^- (dashed curve) versus Φ_{ex} for selected values of junction critical current asymmetry α_i, between 0 and 0.95, calculated with $\beta_l = 0.0098$ and $n = 36$. (b) Rectification coefficient η versus Φ_{ex} calculated for the same values of α_i selected for (a). (c) Maximum rectification efficiency η_M versus α_i (solid violet curve) and asymmetry α_l of the inductance of SQUID arms (dashed pink curve).

It has been previously mentioned that α_L does not significantly impact the device properties. This has been confirmed by the plot of $\eta_M(\alpha_L)$ shown in Fig. 5(c) (dashed-pink line). This is because an asymmetry in the inductance of the two arms of the SQUID loop has the same mathematical effect as a variation of the mutual inductance. With the values selected for n and β_l, the variation of the mutual inductance is negligible. Therefore, even at high inductance asymmetries, there is only a slight modification of the magnetic backaction, which is not perceptible. This makes the device extremely robust to fluctuations in this parameter.

So far, we have assumed the BS SQUID to be realized using ideal tunnel JJ, where the Josephson current is proportional to the sine of the phase difference between the superconducting leads. Higher-order harmonics should be included in the formulation of the JJ current-phase relation [72,73], to consider additional effects such as pair-breaking mechanisms and the proximity effect between the banks [74–77] or to extend our formulation to more complicated types of Josephson junctions (including nanoconstrictions realized through Dayem bridges or superconductor-normal metal-superconductor junctions with a normal metal as a weak link) [74,75]. The current-phase relation of these weak links deviates significantly from the simple sinusoidal form, and it is expected to severely impact the rectification performance of the BS SQUID due to a SQUID current-flux relation, which is always significantly different from 0. This can be qualitatively understood by considering that each spectral component of the current flux relation vanishes at a different value of the magnetic flux. To include this mechanism in our discussion, we calculated the response of a BS SQUID in which the tunnel JJs are replaced by two diffusive short constrictions obeying the Kulik-Omel'yanchuk (KO-1) model [74,75] [i.e., superconductor-constriction-superconductor (*S*-*C*-*S*) JJs], which allowed us to express the switching current of the junctions as

$$I_{L,R}(\varphi_{L,R}, T) = \frac{\pi\Delta(T)}{eR_N}\cos\left(\frac{\varphi_{L,R}}{2}\right) \times \int_{\Delta(T)\cos(\varphi_{L,R}/2)}^{\Delta(T)} \frac{\tanh\left(\frac{\varepsilon}{k_BT}\right)}{\sqrt{\varepsilon^2 - \Delta^2(T)\cos^2(\varphi_{L,R}/2)}}d\varepsilon, \quad (5)$$

where e is the electron charge, and R_N is the junction normal-state resistance, which we assume to be the same for the left and right junctions. Although this formulation is valid only in the dirty and short constriction limit, the behavior described and the conclusion drawn in the following are expected to qualitatively remain valid for any junction characterized by a nonmonochromatic current-phase relation.

Figure 6(a) shows the positive and the negative switching currents versus external magnetic flux at selected values of T of a BS SQUID with $\beta_{l0} = 0.0098$ and $n = 36$ based on SCS JJs, as depicted in the inset of Fig. 6(b). Due to the $I_{L,R}(T)$ characteristics of the weak links [see Fig. 6(c), black-dashed curve], the amplitude of the switching current modulation remains constant up to approximately $0.4T_C$, above this threshold it decreases to vanish at T_C. Furthermore, due to the KO-1 current-phase relation recovering a quasisinusoidal behavior approaching T_C, the skewness of the $I^{+,-}(\Phi_{ex})$ is partially reabsorbed as the temperature increases. Similarly to the tunnel junction case, the temperature evolution of η, plotted versus Φ_{ex} in Fig. 6(b) for the same selected values of T of (a), is determined by the double impact of the reduction of $I_{L,R}$ on both the maxima of $|I_S^{+,-}|$ and on β_l: the pattern of η remains essentially unchanged as the temperature rises to approximately $0.5T_C$, but, above this threshold, its amplitude monotonically decreases. As discussed, η_M [see Fig. 6(c), red-solid curve] is always very far from the near-ideal rectification case, reaching its maximum value of approximately 0.6 when T vanishes. Still remarkable, this value is much lower than that obtained with sinusoidal junctions, suggesting the latter as the ideal platform for implementing the BS SQUID.

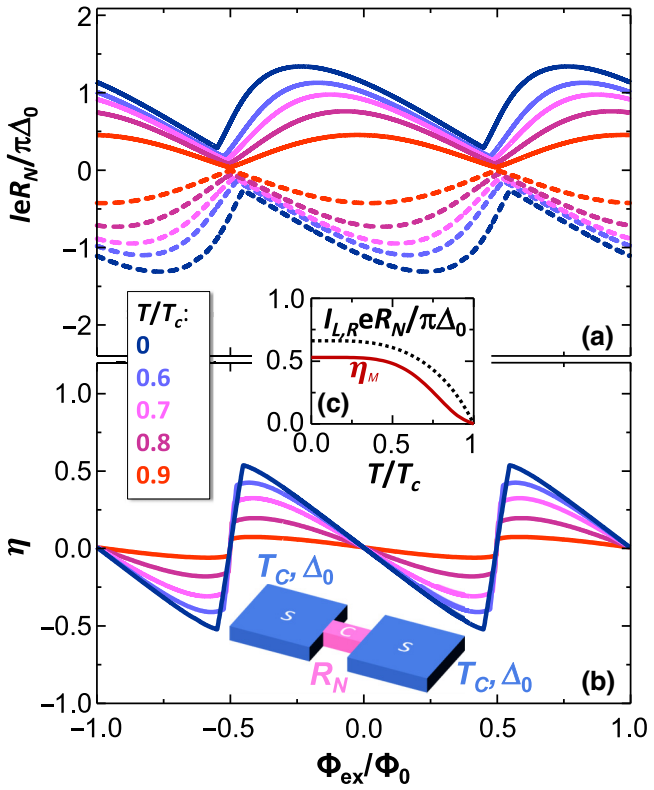

FIG. 6. BS-SQUID realized through diffusive short constrictions. (a) I^+ (solid curves) and I^- (dashed curves) versus Φ_{ex} for selected values of the temperature T, between 0 and 0.9 T_C, calculated for a perfectly symmetrical BS SQUID with $\beta_{l0} = 0.0098$ and $n = 36$. The junction current phase relation adopted for this calculation is the KO-1. (b) Rectification coefficient η versus Φ_{ex} for the same values of T selected for (a). Inset: scheme of superconductor-constriction-superconductor (S-C-S) Josephson junction. The constriction is assumed to have a normal-state resistance R_N, equal for both the SQUID junctions. The amplitude of the superconducting gap and of the critical temperature of the S leads is assumed to be Δ_0 and T_C, respectively. (c) Maximum rectification coefficient η_M (solid red curve) and Josephson critical current $I_{L,R}$ (black dashed line) versus temperature T.

V. DISSIPATIVE OPERATION

Practical dc SQUIDs are conventionally operated in a dissipative fashion, as they are usually biased close to or above their critical current. That is, the SQUID is driven in a dissipative or finite-voltage state. In the following, we would like to discuss the response of BS SQUID in such a regime. In this configuration, the SQUID response can be analytically calculated following the relation: [43]

$$\frac{V}{V_0} = \frac{\sqrt{I^2 - 4I_0^2}}{I_0}, \tag{6}$$

where V is the voltage drop across the BS SQUID [see the biasing scheme in Fig. 1(a)], $V_0 = 2R_T I_0$ is a critical voltage, calculated through the tunnel resistance R_T of the JJs. Equation (6) holds in the limit $(2\pi/\Phi_0)I_0R_T^2C \ll 1$ [43,78], where C is the capacitance of each JJ. This condition can usually be obtained by adopting shunt resistors with resistance R such as $R < R_T$. In the latter case, V_0 has to be modified accordingly to account for the parallel of the shunt resistor and the JJ.

Figure 7(a) shows in a color plot the voltage response of a BS SQUID versus Φ_{ex} and I, when $n = 36$ and $\beta_l = 0.098$. The aquamarine area corresponds to the nondissipative regime. When the bias current exceeds the positive (yellowish area) or the negative (blueish area) switching current of the BS SQUID, a finite-voltage response is obtained. The region in the (Φ, I) plane where the BS SQUID can be successfully exploited as a tunable supercurrent diode corresponds to the area where, at constant flux, a constant-current cut line can cross the boundary between dissipative and nondissipative operation [dashed-white boundary in Fig. 7(a)]. When this condition is not fulfilled, the device is either always superconducting or

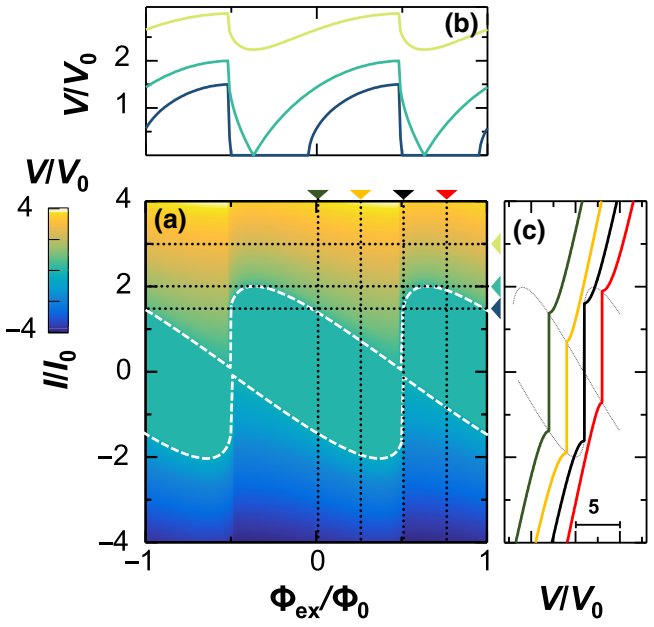

FIG. 7. BS SQUID response in the dissipative regime. (a) Normalized voltage drop of a BS SQUID versus Φ_{ex} and bias current I, calculated for a perfectly symmetric device with $\beta_l = 0.0098$ and $n = 36$. The superconducting phase can be identified by the zero-voltage region colored in aquamarine and bounded by the white-dashed lines. Dashed-black lines correspond to the curves at constant current or constant flux, plotted in (b),(c), respectively. The color of the markers at the edge of the color plot identifies the curve in (b),(c) with the same colors. (b) V versus Φ_{ex} curves for selected values of I corresponding to the cut lines at constant current (a). (c) V versus I curves for selected values of Φ_{ex}, corresponding to the cut lines at constant flux of (a). For the sake of clarity, the curves are horizontally offset by a quantity proportional to the correspondent flux. The dashed gray lines guide the eye, which follow the evolution of I^+ and I^- with Φ_{ex}.

resistive. The cut lines of the color plot at selected values of the constant current are shown in Fig. 7(b): due to the skewed nature of the $I^{+,-}(\Phi_{ex}$ of the BS SQUID, the voltage response is very far from the quasisinusoidal behavior of a conventional SQUID. This feature is usually conveniently exploited in the feedback loop SQUID [52–60] to enhance the device transfer function $\partial V/\partial\Phi_{ex}$. From this point of view, the BS SQUID is equivalent to a conventional additional positive feedback superconducting interferometer. The cut lines of the color plot at selected values of Φ_{ex}, shown in Fig. 7(c), on the other hand, allow us to appreciate the tunability of the BS SQUID as a supercurrent diode. These curves, indeed, represent the current-voltage characteristics $(I - V)$ of the device at selected values of the external flux. The net effect of sweeping the latter is equivalent to a shift in the current of device $I - V$. This mechanism can indeed be exploited to tune and reverse the polarity of the diode effect.

We can discuss a practical application of a supercurrent rectifier based on the BS SQUID scheme. Specifically, we focus on rectifying a sinusoidal signal applied as a current bias to the device. This use case involves the detection of a radio-frequency signal collected through a superconducting antenna and rectified through the BS SQUID. A generic monochromatic current signal can be written as $I = I_{mod}\sin((2\pi t)/f)$, where f is the signal frequency, t is the time coordinate, and I_{mod} is the peak-to-peak amplitude of the signal [see Fig. 8(a)]. We can model the temporal output of the BS SQUID using Eq. (6). Figure 8(b) displays $V(T)$ for selected values of I_{mod} when $\beta_l = 0.098$, $n = 36$, and $\phi_{ex} = 0.52\Phi_0$. With the chosen parameters, the BS SQUID exhibits quasi-ideal rectification ability that can efficiently rectify the signal up to $I_{mod} \lesssim 1.6I_0$. However, beyond this threshold, a dissipative regime occurs

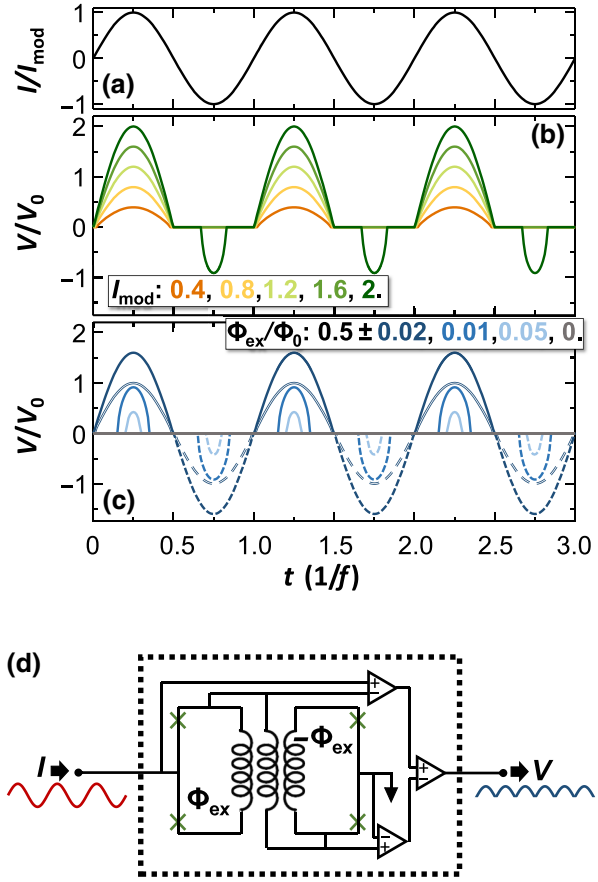

FIG. 8. Half-wave supercurrent rectification. (a) Normalized sinusoidal current-bias signal versus time t (normalized on signal period $1/f$), applied to a BS SQUID to calculate its time-resolved response. (b) Normalized voltage drop V of a perfectly symmetric BS SQUID, with $\beta_l = 0.0098$ and $n = 36$, for selected amplitudes of the ac current bias and $\Phi ex = 0.052$. (c) Normalized voltage drop V for $I_{mod} = 1.6I_0$ and for selected values of Φ_{ex}: solid and dashed curves correspond to positive and negative shifts from $\Phi_{ex} = 0.5$, respectively. (d) Scheme of a possible implementation of a full-wave supercurrent rectifier based on the series of two BS SQUID sharing the same feedback inductance.

in the *reverse* half-period [e.g., the dark green curve in Fig. 8(b)], resulting in a reduction of the net average dc output voltage. By adjusting the flux working point, we can tune the rectification efficiency and eventually reverse the polarity of the diode.

In Fig. 8(c), we can see the output signal of a BS SQUID that operates in the same conditions as the one shown in (b). When we move away from the ideal working point of $\Phi_{ex} \sim (0.5 \pm 0.02)\Phi_0$, the fraction of the rectified signal is reduced. Crossing the value of $0.5\Phi_0$ reverses the polarity of the diode [as seen in the dashed curves in Fig. 8(a)], allowing the rectification of the second half-period of the signal. Based on this observation, we can say that coupling two SQUIDs to the same feedback loop, as shown in Fig. 8(d), can help us realize a full-wave rectifier without increasing the inductance of the device significantly. This observation is particularly relevant because the feedback inductor and the tunnel resistance impact the device's cutoff frequency of operation due to its reactive behavior. Assuming $n = 36$ and $d = 1$ μm, we can estimate $L_S \simeq 1.6$ pH and $L_F \simeq 2$ nH. To maximize η by assuming $\beta_l \sim 0.01$, I_0 needs to be approximately 6 μA, which can be routinely obtained with $Al/AlO_x/Al$ JJs by setting a tunnel resistance of approximately 200 Ω during fabrication. The cutoff frequency due to the reactive component of the BS SQUID impedance is, therefore, $f_l = R_t/L_F \sim 100$ GHz. Assuming a junction area of the order of 2 μm^2, we can also estimate the junction capacitance $C \sim 0.2$ pF and the consequent cutoff frequency due to the capacitive impedance $f_C = 1/R_t C \sim 50$ GHz, which results in the most limiting timescale with this parameter choice.

VI. CONCLUSIONS

In summary, we have proposed a SQUID with a feedback loop called the boot-strap SQUID. This device is based on a magnetic flux backaction that produces a robust nonreciprocal current-voltage characteristic. By correctly choosing the external magnetic flux Φ_{ex}, our device can pull the supercurrent rectification coefficient to nearly unit value, resulting in a quasi-ideal supercurrent diode. Additionally, the magnetic flux knob can be utilized to tune and reverse the supercurrent rectification polarity. We discussed the temperature evolution of the BS SQUID architecture and its resilience to fabrication imperfections. We also presented a possible use case as a half- or full-wave signal rectifier with a cutoff frequency of a few tens of GHz.

ACKNOWLEDGMENTS

We acknowledge the EU's Horizon 2020 Research and Innovation Framework Programme under Grants No. 964398 (SUPERGATE), No. 101057977 (SPECTRUM), and the PNRR MUR project PE0000023-NQSTI for partial financial support.

[1] D. A. Buck, The cryotron - a superconductive computer component, Proc. IRE **44**, 482 (1956).
[2] A. N. McCaughan and K. K. Berggren, Superconducting-nanowire three-terminal electrothermal device, Nano Lett. **14**, 5784 (2014).
[3] K. K. Likharev and V. K. Semenov, RSFQ logic/memory family: A new Josephson-junction technology for sub-terahertz-clock-frequency digital systems, IEEE Trans. Appl. Supercond. **1**, 3 (1991).
[4] T. Nishino, M. Hatano, H. Hasegawa, F. Murai, T. Kure, A. Hiraiwa, K. Yagi, and U. Kawabe, 0.1-mu m gate-length superconducting FET, IEEE Electron Device Lett. **10**, 61 (1989).
[5] T. D. Clark, R. J. Prance, and A. D. C. Grassie, Feasibility of hybrid Josephson field effect transistors, J. Appl. Phys. **51**, 2736 (1980).
[6] G. De Simoni, F. Paolucci, P. Solinas, E. Strambini, and F. Giazotto, Metallic supercurrent field-effect transistor, Nat. Nanotechnol. **13**, 802 (2018).
[7] M. F. Ritter, A. Fuhrer, D. Z. Haxell, S. Hart, P. Gumann, H. Riel, and F. Nichele, A superconducting switch actuated by injection of high-energy electrons, Nat. Commun. **12**, 1266 (2021).
[8] O.-A. Adami, D. Cerbu, D. Cabosart, M. Motta, J. Cuppens, W. A. Ortiz, V. V. Moshchalkov, B. Hackens, R. Delamare, J. Van de Vondel, and A. V. Silhanek, Current crowding effects in superconducting corner-shaped Al microstrips, Appl. Phys. Lett. **102**, 052603 (2013).
[9] Fuyuki Ando, Yuta Miyasaka, Tian Li, Jun Ishizuka, Tomonori Arakawa, Yoichi Shiota, Takahiro Moriyama, Youichi Yanase, and Teruo Ono, Observation of superconducting diode effect, Nature **584**, 373 (2020).
[10] Ryohei Wakatsuki, Yu Saito, Shintaro Hoshino, Yuki M. Itahashi, Toshiya Ideue, Motohiko Ezawa, Yoshihiro Iwasa, and Naoto Nagaosa, Nonreciprocal charge transport in noncentrosymmetric superconductors, Sci. Adv. **3**, e1602390 (2017).
[11] J. Díez-Mérida, A. Díez-Carlón, S. Y. Yang, Y.-M. Xie, X.-J. Gao, J. Senior, K. Watanabe, T. Taniguchi, X. Lu, and Andrew P. Higginbotham *et al.*, Symmetry-broken Josephson junctions and superconducting diodes in magic-angle twisted bilayer graphene, Nat. Commun. **14**, 2396 (2023).
[12] Jiang-Xiazi Lin, Phum Siriviboon, Harley D. Scammell, Song Liu, Daniel Rhodes, K. Watanabe, T. Taniguchi, James Hone, Mathias S. Scheurer, and J. I. A. Li, Zero-field superconducting diode effect in small-twist-angle trilayer graphene, Nat. Phys. **18**, 1221 (2022).
[13] Banabir Pal, Anirban Chakraborty, Pranava K. Sivakumar, Margarita Davydova, Ajesh K. Gopi, Avanindra K. Pandeya, Jonas A. Krieger, Yang Zhang, Mihir Date, and Sailong Ju *et al.*, Josephson diode effect from cooper pair momentum in a topological semimetal, Nat. Phys. **18**, 1228 (2022).
[14] Lorenz Bauriedl, Christian Bäuml, Lorenz Fuchs, Christian Baumgartner, Nicolas Paulik, Jonas M. Bauer, Kai-Qiang Lin, John M. Lupton, Takashi Taniguchi, and Kenji Watanabe *et al.*, Supercurrent diode effect and magnetochiral anisotropy in few-layer $NbSe_2$, Nat. Commun. **13**, 4266 (2022).
[15] Christian Baumgartner, Lorenz Fuchs, Andreas Costa, Simon Reinhardt, Sergei Gronin, Geoffrey C. Gardner,

Tyler Lindemann, Michael J. Manfra, Paulo E. Faria Junior, and Denis Kochan *et al.*, Supercurrent rectification and magnetochiral effects in symmetric Josephson junctions, Nat. Nanotechnol. **17**, 39 (2022).

[16] Kun-Rok Jeon, Jae-Keun Kim, Jiho Yoon, Jae-Chun Jeon, Hyeon Han, Audrey Cottet, Takis Kontos, and Stuart S. P. Parkin, Zero-field polarity-reversible Josephson supercurrent diodes enabled by a proximity-magnetized Pt barrier, Nat. Mater. **21**, 1008 (2022).

[17] Ananthesh Sundaresh, Jukka I. Väyrynen, Yuli Lyanda-Geller, and Leonid P. Rokhinson, Diamagnetic mechanism of critical current non-reciprocity in multilayered superconductors, Nat. Commun. **14**, 1628 (2023).

[18] Bianca Turini, Sedighe Salimian, Matteo Carrega, Andrea Iorio, Elia Strambini, Francesco Giazotto, Valentina Zannier, Lucia Sorba, and Stefan Heun, Josephson diode effect in high-mobility InSb nanoflags, Nano Lett. **22**, 8502 (2022).

[19] Akito Daido, Yuhei Ikeda, and Youichi Yanase, Intrinsic superconducting diode effect, Phys. Rev. Lett. **128**, 037001 (2022).

[20] M. Nadeem, M. S. Fuhrer, and X. Wang, The superconducting diode effect, Nat. Rev. Phys. **5**, 558 (2023).

[21] Stefan Ilić and F. Sebastian Bergeret, Theory of the supercurrent diode effect in Rashba superconductors with arbitrary disorder, Phys. Rev. Lett. **128**, 177001 (2022).

[22] Noah F. Q. Yuan and Liang Fu, Supercurrent diode effect and finite-momentum superconductors, Proc. Natl. Acad. Sci. **119**, e2119548119 (2022).

[23] James Jun He, Yukio Tanaka, and Naoto Nagaosa, A phenomenological theory of superconductor diodes, New J. Phys. **24**, 053014 (2022).

[24] Kou Misaki and Naoto Nagaosa, Theory of the nonreciprocal Josephson effect, Phys. Rev. B **103**, 245302 (2021).

[25] Margarita Davydova, Saranesh Prembabu, and Liang Fu, Universal Josephson diode effect, Sci. Adv. **8**, eabo0309 (2022).

[26] Yi Zhang, Yuhao Gu, Pengfei Li, Jiangping Hu, and Kun Jiang, General theory of Josephson diodes, Phys. Rev. X **12**, 041013 (2022).

[27] Harley D. Scammell, J. I. A. Li, and Mathias S. Scheurer, Theory of zero-field superconducting diode effect in twisted trilayer graphene, 2D Mater. **9**, 025027 (2022).

[28] J. F. Wambaugh, C. Reichhardt, C. J. Olson, F. Marchesoni, and Franco Nori, Superconducting fluxon pumps and lenses, Phys. Rev. Lett. **83**, 5106 (1999).

[29] D. Yu Vodolazov and F. M. Peeters, Superconducting rectifier based on the asymmetric surface barrier effect, Phys. Rev. B **72**, 172508 (2005).

[30] J. E. Villegas, E. M. Gonzalez, M. P. Gonzalez, José Virgilio Anguita, and J. L. Vicent, Experimental ratchet effect in superconducting films with periodic arrays of asymmetric potentials, Phys. Rev. B **71**, 024519 (2005).

[31] Joris Van de Vondel, C. C. de Souza Silva, B. Y. Zhu, Mathieu Morelle, and V. V. Moshchalkov, Vortex-rectification effects in films with periodic asymmetric pinning, Phys. Rev. Lett. **94**, 057003 (2005).

[32] Dorin Cerbu, V. N. Gladilin, Johan Cuppens, Joachim Fritzsche, Jacques Tempere, J. T. Devreese, V. V. Moshchalkov, A. V. Silhanek, and Joris Van de Vondel, Vortex ratchet induced by controlled edge roughness, New J. Phys. **15**, 063022 (2013).

[33] Taras Golod, Razmik A. Hovhannisyan, Olena M. Kapran, Vyacheslav V. Dremov, Vasily S. Stolyarov, and Vladimir M. Krasnov, Reconfigurable Josephson phase shifter, Nano Lett. **21**, 5240 (2021).

[34] Yang-Yang Lyu, Ji Jiang, Yong-Lei Wang, Zhi-Li Xiao, Sining Dong, Qing-Hu Chen, Milorad V. Milošević, Huabing Wang, Ralu Divan, and John E. Pearson *et al.*, Superconducting diode effect via conformal-mapped nanoholes, Nat. Commun. **12**, 2703 (2021).

[35] Taras Golod and Vladimir M. Krasnov, Demonstration of a superconducting diode-with-memory, operational at zero magnetic field with switchable nonreciprocity, Nat. Commun. **13**, 3658 (2022).

[36] Dhavala Suri, Akashdeep Kamra, Thomas N. G. Meier, Matthias Kronseder, Wolfgang Belzig, Christian H. Back, and Christoph Strunk, Non-reciprocity of vortex-limited critical current in conventional superconducting microbridges, Appl. Phys. Lett. **121**, 102601 (2022).

[37] Sara Chahid, Serafim Teknowijoyo, Iris Mowgood, and Armen Gulian, High-frequency diode effect in superconducting Nb_3Sn microbridges, Phys. Rev. B **107**, 054506 (2023).

[38] Yasen Hou, Fabrizio Nichele, Hang Chi, Alessandro Lodesani, Yingying Wu, Markus F. Ritter, Daniel Z. Haxell, Margarita Davydova, Stefan Ilić, and Ourania Glezakou-Elbert *et al.*, Ubiquitous superconducting diode effect in superconductor thin films, Phys. Rev. Lett. **131**, 027001 (2023).

[39] N. Satchell, P. M. Shepley, M. C. Rosamond, and G. Burnell, Supercurrent diode effect in thin film Nb tracks, J. Appl. Phys. **133**, 203901 (2023).

[40] Ondrej Vavra, Wolfgang Pfaff, R. Monaco, M. Aprili, and Christoph Strunk, Current-controllable planar s-(s/f)-s Josephson junction, Appl. Phys. Lett. **102**, 072602 (2013).

[41] Daniel Margineda, Alessandro Crippa, Alessandro Strambini, Yuri Fukaya, Maria Teresa Mercaldo, Mario Cuoco, and Francesco Giazotto, Sign reversal diode effect in superconducting Dayem nanobridges, Commun. Phys. **6**, 343 (2023).

[42] Daniel Margineda, Alessandro Crippa, Elia Strambini, Yuri Fukaya, Maria Teresa Mercaldo, Carmine Ortix, Mario Cuoco, and Francesco Giazotto, Back-action supercurrent diodes, arXiv:2311.14503v2 (2023).

[43] John Clarke and Alex I. Braginski, *The SQUID Handbook*, edited by John Clarke and Alex I. Braginski (Wiley, Weinhei, 2004), Vol. 1, p. 1.

[44] Antonio Barone and Gianfranco Paternò, *Physics and Applications of the Josephson Effect* (John Wiley & Sons, Inc, New York, 1982).

[45] R. Kleiner, D. Koelle, F. Ludwig, and J. Clarke, Superconducting quantum interference devices: State of the art and applications, Proc. IEEE **92**, 1534 (2004).

[46] Maria José Martínez-Pérez and Dieter Koelle, in *Superconductors at the Nanoscale: From Basic Research to Applications*, edited by Roger Wördenweber, Victor Moshchalkov, Simon Bending, and Francesco Tafuri (De Gruyter, Berlin/Boston, 2017), p. 339.

[47] Carmine Granata and Antonio Vettoliere, Nano superconducting quantum interference device: A powerful tool for nanoscale investigations, Phys. Rep. **614**, 1 (2016).

[48] Robert L. Fagaly, Hans-Joachim Krause, Michael Mück, Saburo Tanaka, Hannes Nowak, Ronny Stolz, John Kirtley, Thomas Schurig, Jörn Beyer, Robert McDermott, Wolfgang Vodel, Rene Geithner, and Paul Seidel, in *Applied Superconductivity* (John Wiley & Sons, Ltd, Weinhei, 2015), Chap. 9, p. 949.

[49] V. K. Kornev, N. V. Kolotinskiy, A. V. Sharafiev, I. I. Soloviev, and O. A. Mukhanov, From single SQUID to superconducting quantum arrays, Low Temp. Phys. **43**, 829 (2017).

[50] F. Paolucci, G. De Simoni, and F. Giazotto, A gate-and flux-controlled supercurrent diode effect, Appl. Phys. Lett. **122**, 042601 (2023).

[51] A. Greco, Q. Pichard, and F. Giazotto, Josephson diode effect in monolithic dc-SQUIDs based on 3D Dayem nanobridges, Appl. Phys. Lett. **123**, 092601 (2023).

[52] D. Drung, R. Cantor, M. Peters, H. J. Scheer, and H. Koch, Low-noise high-speed dc superconducting quantum interference device magnetometer with simplified feedback electronics, Appl. Phys. Lett. **57**, 406 (1990).

[53] Michael Mück, Increasing the dynamic range of a SQUID amplifier by negative feedback, Phys. C: Supercond. **368**, 141 (2002).

[54] H. Seppa, A. Ahonen, J. Knuutila, J. Simola, and V. Volkman, Dc-SQUID electronics based on adaptive positive feedback: Experiments, IEEE Trans. Magn. **27**, 2488 (1991).

[55] Dietmar Drung, Low-frequency noise in low-T_c multiloop magnetometers with additional positive feedback, Appl. Phys. Lett. **67**, 1474 (1995).

[56] Mikko Kiviranta and Heikki Seppä, Dc-SQUID electronics based on the noise cancellation scheme, IEEE Trans. Appl. Supercond. **5**, 2146 (1995).

[57] Mikko Kiviranta, SQUID linearization by current-sampling feedback, Supercond. Sci. Technol. **21**, 045009 (2008).

[58] Xiaoming Xie, Yi Zhang, Huiwu Wang, Yongliang Wang, Michael Mück, Hui Dong, Hans-Joachim Krause, Alex I. Braginski, Andreas Offenhäusser, and Mianheng Jiang, A voltage biased superconducting quantum interference device bootstrap circuit, Supercond. Sci. Technol. **23**, 065016 (2010).

[59] Huiwu Wang, Yongliang Wang, Hui Dong, Yi Zhang, Xiaoming Xie, Hans-Joachim Krause, and Andreas Offenhäusser, Noise behavior of SQUID bootstrap circuit studied by numerical simulation, Phys. Procedia **36**, 127 (2012). Superconductivity Centennial Conference 2011.

[60] Guo-Feng Zhang, Yi Zhang, Hans-Joachim Krause, Xiang-Yan Kong, Andreas Offenhäusser, and Xiao-Ming Xie, A SQUID bootstrap circuit with a large parameter tolerance, Chin. Phys. Lett. **30**, 018501 (2013).

[61] Giorgio De Simoni and Francesco Giazotto, Ultralinear magnetic-flux-to-voltage conversion in superconducting quantum interference proximity transistors, Phys. Rev. Appl. **19**, 054021 (2023).

[62] Giorgio De Simoni, Lorenzo Cassola, Nadia Ligato, Giuseppe C. Tettamanzi, and Francesco Giazotto, Ultra-high linearity of the magnetic-flux-to-voltage response of proximity-based mesoscopic bi-SQUIDs, Phys. Rev. Appl. **18**, 014073 (2022).

[63] M. B. Ketchen and J. M. Jaycox, Ultra-low-noise tunnel junction dc SQUID with a tightly coupled planar input coil, Appl. Phys. Lett. **40**, 736 (1982).

[64] J. Jaycox and M. Ketchen, Planar coupling scheme for ultra low noise dc SQUIDs, IEEE Trans. Magn. **17**, 400 (1981).

[65] Neda Lotfizadeh, William F. Schiela, Barış Pekerten, Peng Yu, Bassel Heiba Elfeky, William M. Strickland, Alex Matos-Abiague, and Javad Shabani, Superconducting diode effect sign change in epitaxial Al-InAs Josephson junctions, Commun. Phys. **7**, 120 (2024).

[66] A. Costa, C. Baumgartner, S. Reinhardt, J. Berger, S. Gronin, G. C. Gardner, T. Lindemann, M. J. Manfra, J. Fabian, D. Kochan, N. Paradiso, and C. Strunk, Sign reversal of the Josephson inductance magnetochiral anisotropy and 0-π-like transitions in superconducting diodes, Nat. Nanotechnol. **18**, 1266 (2023).

[67] Ryo Kawarazaki, Hideki Narita, Yuta Miyasaka, Yuhei Ikeda, Ryusuke Hisatomi, Akito Daido, Yoichi Shiota, Takahiro Moriyama, Youichi Yanase, and Alexey V. Ognev *et al.*, Magnetic-field-induced polarity oscillation of superconducting diode effect, Appl. Phys. Express **15**, 113001 (2022).

[68] Mohit Gupta, Gino V. Graziano, Mihir Pendharkar, Jason T. Dong, Connor P. Dempsey, Chris Palmstrøm, and Vlad S. Pribiag, Gate-tunable superconducting diode effect in a three-terminal Josephson device, Nat. Commun. **14**, 3078 (2023).

[69] V. Ambegaokar and A. Baratoff, Tunneling between superconductors, Phys. Rev. Lett. **10**, 486 (1963).

[70] V. Ambegaokar and A. Baratoff, Erratum: Tunneling between superconductors, Phys. Rev. Lett. **11**, 104 (1963).

[71] Michael Tinkham, *Introduction to Superconductivity* (Courier Corporation, New York, 2004).

[72] A. S. Osin and Ya. V. Fominov, Superconducting phases and the second Josephson harmonic in tunnel junctions between diffusive superconductors, Phys. Rev. B **104**, 064514 (2021).

[73] Dennis Willsch *et al.*, Observation of Josephson harmonics in tunnel junctions, Nat. Phys. **20**, 815 (2024).

[74] A. A. Golubov, M. Yu. Kupriyanov, and E. Il'ichev, The current-phase relation in Josephson junctions, Rev. Mod. Phys. **76**, 411 (2004).

[75] K. K. Likharev, Superconducting weak links, Rev. Mod. Phys. **51**, 101 (1979).

[76] Yu. S. Barash, Anharmonic Josephson current in junctions with an interface pair breaking, Phys. Rev. B **85**, 100503 (2012).

[77] Yu S. Barash, Interfacial pair breaking and planar weak links with an anharmonic current-phase relation, JETP Lett. **100**, 205 (2014).

[78] D. E. McCumber, Effect of ac impedance on dc voltage-current characteristics of superconductor weak-link junctions, J. Appl. Phys. **39**, 3113 (1968).